A&A 417, 39–50 (2004)
DOI: 10.1051/0004-6361:20035602

Astronomy & Astrophysics

Dust masses and star formation in bright IRAS galaxies

Application of a physical model for the interpretation of FIR observations

A. Misiriotis[1], I. E. Papadakis[1,2], N. D. Kylafis[1,2], and J. Papamastorakis[1,2]

[1] University of Crete, Physics Department, PO Box 2208, 710 03 Heraklion, Crete, Greece
[2] Foundation for Research and Technology-Hellas, PO Box 1527, 711 10 Heraklion, Crete, Greece

Received 30 October 2003 / Accepted 3 December 2003

Abstract. We address the problem of modeling the far-infrared (FIR) spectrum and deriving the star-formation rate (SFR) and the dust mass of spiral galaxies. We use the realistic physical model of Popescu et al. (2000) to describe the overall ultra-violet (UV), optical and FIR spectral energy distribution (SED) of a spiral galaxy. The model takes into account the 3-dimensional old and young stellar distributions in the bulge and the disk of a galaxy, together with the dust geometry. The geometrical characteristics of the galaxy and the intrinsic optical and near-infrared spectra are determined by the galaxy's observed K-band photometry. The UV part of the spectrum is assumed to be proportional to the SFR through the use of population synthesis models. By solving the radiative transfer equation, we are able to determine the absorbed energy, the dust temperature and the resulting FIR spectrum. The model has only three free parameters: SFR, dust mass, and the fraction of the UV radiation which is absorbed locally by dense dust in the HII regions. Using this model, we are able to fit well the FIR spectra of 62 bright IRAS galaxies from the "SCUBA Local Universe Galaxy Survey" of Dunne et al. (2000). As a result, we are able to determine, among others, their SFR and dust mass. We find that, on average, the SFR (in absolute units), the star-formation efficiency, the SFR surface density and the ratio of FIR luminosity over the total intrinsic luminosity, are larger than the respective values of typical spiral galaxies of the same morphological type. We also find that the mean gas-to-dust mass ratio is close to the Galactic value, while the average central face-on optical depth of these galaxies in the V band is 2.3. Finally, we find a strong correlation between SFR or dust mass and observed FIR quantities like total FIR luminosity or FIR luminosity at 100 and 850 μm. These correlations yield well-defined relations, which can be used to determine a spiral galaxy's SFR and dust-mass content from FIR observations.

Key words. dust, extinction – galaxies: stellar content – galaxies: ISM – infrared: galaxies

1. Introduction

The galactic environment is a complicated mixture of stars, gas and dust. Stars originate from gas while the presence of dust catalyzes the process. In turn the dust absorbs the light of the stars (new-born and old) to emit the absorbed energy in the far infrared. The relation between star formation, gas and dust is of indispensable importance in any attempt to understand the evolution of galaxies (see Calzetti 2001 for a review on the subject). Thus, a reliable method to determine the SFR has been among the main goals of research the last few years. A plethora of diagnostics have been introduced (see Kennicutt 1998b for a review) to address the problem of deriving an estimate for the SFR of a given galaxy. One of the main problems of most methods is the attenuation from dust that obscures the measured quantities in the UV and optical bands. For example, Charlot et al. (2002), using a combination of population synthesis models and a photoionization code, concluded that standard estimators based on Hα and [OII] underestimate the SFR by a factor of 3. On the other hand, they find that their SFR estimates agree very well with estimates based on the 60 and 100 μm fluxes, indicating that a promising way to overcome the problem of attenuation of traditional SFR diagnostics is the use of dust emission itself as a SFR diagnostic. This is straightforward in starburst galaxies where the dust opacity is high and most of the dust heating originates from the young stellar population. In this case, the FIR luminosity can be used as a direct measure of the SFR (e.g. Lehnert & Heckman 1996; Meurer et al. 1997)

However, the situation is more complicated in normal spiral galaxies where the stellar luminosity is not completely reprocessed by interstellar dust. For example, Xu & Buat (1995) compared the UV, optical and FIR emission (estimated from IRAS measurements) from a sample of 135 spirals and found that only 30% of the total bolometric luminosity is emitted at the FIR. A more recent work, based on a direct measurement

Send offprint requests to: A. Misiriotis,
e-mail: angmis@physics.uoc.gr

of the bulk of the dust emission[1] was obtained by Popescu & Tuffs (2002) and suggests that the percentage of stellar light re-radiated by dust lies between 15 to 50%.

These studies indicate that the moderate optical depth of normal galaxies allows a significant fraction of the UV radiation to escape the galaxy without heating the dust. Furthermore, a percentage of the dust heating in normal galaxies can be attributed to the old stellar population as well. These two effects complicate the relation between SFR and FIR in these galaxies.

To address properly the relation between SFR and FIR in normal galaxies with moderate optical depth the use of a detailed theoretical model for the FIR emission is required. The origin of the dust heating, the dust mass, and the optical depth are questions entangled in the problem of defining the SFR–FIR relation, and should be addressed simultaneously by the model. The model should also take into account the geometry of the stars (both old and young) and the dust. The radiative transfer equation (RTE) should be solved and the emerging spectrum from the UV to the FIR should be calculated. Comparison of the theoretical SEDs with observed FIR spectra will then allow an accurate investigation of whether and how the various observational properties (i.e. FIR luminosity, flux at certain bands, FIR colors) correlate with the fundamental physical parameters like SFR and dust mass.

A few authors have followed this approach in the past. For example, Buat & Xu (1996) (see also Buat et al. 2002) compared the UV with the FIR emission of 152 disk galaxies. They used a simplified model to calculate the extinction at the UV band. Given the extinction they corrected the UV emission and calibrated the FIR luminosity in terms of SFR. In the same fashion, Hirashita et al. (2003) derived extinction correction for several SFR indicators based on the simple assumption that all the estimators should return the same SFR. They applied their method on a sample of 47 irregulars and spirals and 32 starburst galaxies and emphasized the role of dust extinction on several SFR tracers. Bianchi et al. (2000) used a detailed Monte Carlo radiative transfer code and applied it to one object, namely NGC 6946. They used this code to model its overall SED, and concluded that it's central face-on optical depth is of the order of 5. According to the predictions of their model, the old stellar population is the main source of dust heating and therefore they draw no conclusions on the SFR of this galaxy. The intrinsic colors of a stellar population depend on the star-formation history of this population. Therefore several authors (e.g. Silva et al. 1998; Devriendt et al. 1999; Efstathiou & Rowan-Robinson 2003) have introduced population synthesis models to describe the intrinsic SEDs of their models and subsequently applied extinction and emission from dust to derive the emerging SED. Yet, these models tend to involve too many parameters that can not be strictly constrained.

Finally, Popescu et al. (2000; P00 hereafter) developed the detailed theoretical model which we use in this paper and which was first tested and applied to the edge-on spiral NGC 891. In their work, they used a detailed geometric description of the galaxy based on optical observations from Xilouris et al. (1998). They also included the effect of localized absorption of the UV in star forming regions. They found that 30% of the dust heating is attributed to the old stellar population. The model of P00 was successful not only in fitting the SED of NGC 891 but also in predicting the FIR morphology of this galaxy (Popescu et al. 2003).

Furthermore, the same model was applied on 4 more edge-on galaxies by Misiriotis et al. (2001) to derive their SFR and dust mass. Their results are in excellent agreement with the SFRs derived by Kennicutt (1998a) from a sample of 61 normal spiral galaxies.

Since FIR observations that cover the full range from 10 to 1000 μm are becoming rapidly available, it is desirable to develop a method which will allow us to use these observations to derive important physical parameters of spiral galaxies, such as the SFR and the dust mass. In this paper we present the first application of the P00 model to a large number of spiral galaxies with IRAS data and recent high quality FIR measurements (Dunne et al. 2000; DU00 hereafter). The use of a realistic physical model and the excellent agreement between the model SEDs and the FIR measurements, allow us to derive reliable SFR and dust-mass values. Furthermore, the large number of galaxies considered in this work allows us to detect significant correlations and derive important diagnostic relations between various observational FIR emission properties and these physical parameters.

In Sect. 2 we discuss the physical model for the FIR emission that we are using. In Sect. 3 we present the data for the sample of galaxies we consider in this study, and in Sect. 4 we describe the fitting procedure of our model SEDs to the observed FIR spectra. In Sect. 5 we present and discuss the results from the model fitting procedure, namely the SFRs and the dust masses for the galaxies in our sample. In Sect. 6 we show diagnostic relations that we derived between measured FIR and physical quantities, and we summarize in Sect. 7.

2. Description of the FIR emission model

The model used in this work is based on the model of P00, to which the reader should refer for more details. Two simplifications were made due to the statistical character of this study.

1. In P00 the dust is distributed in two exponential disks with different scalelengths and scaleheights. This detailed approach was directed by the large amount of data available for NGC 891. In this study such data are not available and therefore only one exponential disk is used to describe the dust distribution;
2. in P00 the stochastic heating of the diffuse dust was taken into account. In the present work, the stochastic heating was neglected due to the computational load it would require.

In the rest of this section we will present an outline of the model and discuss the assumptions we made due to the lack of detailed data for our sample. Our primary aim is to construct a theoretical model which will allow us to reproduce reliably the overall UV, optical and FIR SED emerging from a spiral galaxy. To this end, one has to determine the intrinsic luminosity of a galaxy in several wavelengths as well as the parameters describing the spatial distribution of the stars (e.g. the

[1] Using ISO data from Tuffs et al. (2002).

disk and bulge scalelengths, scaleheights etc.) and dust. Then, given the stellar and dust spatial distributions, one has to solve the RTE. The solution of the RTE provides among others the absorbed energy that heats the dust. At the same time, the extinction effects in the UV and the optical part of the SED are calculated. According to the dust's temperature and emission properties, the absorbed energy is re-emitted in the FIR. Since the absorbed energy varies from point to point, the RTE must be solved for a grid within the model galaxy. Then, the dust emission from all the grid points is integrated to get the total emission spectrum of the dust.

For edge-on spiral galaxies, the parameters which determine the geometry of stars and dust can be found using the method introduced by Kylafis & Bahcall (1987) and subsequently used by Ohta & Kodaira (1995), Xilouris et al. (1997, 1998, 1999), Kuchinski et al. (1998). This method consists of finding a 3D distribution for the stars and the dust that replicates the actual observed image of the galaxy. The prominent dust lane in edge-on galaxies constrains the dust mass as well as it's scalelength and scaleheight.

However, the observational determination of all the photometric and geometric parameters is not possible for the majority of the spiral galaxies, which are not seen edge-on. In this case, one has to assume the 3D stellar and dust distributions, based on the results from 2D bulge-disk decomposition studies. In our case we choose to represent a spiral galaxy using an exponential stellar disk, an oblate exponential bulge with axial ratio 0.5 and an exponential dust disk.

2.1. Spatial distribution of the old stellar population

In order to determine the geometric parameters of the stellar distribution in a galaxy we use mainly the results of de Jong (1996; DJ96 hereafter), which are based on optical and near-infrared observations of 86 face-on spiral galaxies. We start by determining the scalelength, h_s (in pc), of the disk (which represents the old stellar population) with the use of the relation: $M_{K,d} = -6-5\log(h_s)$, where $M_{K,d}$ is the K-band absolute magnitude of the disk. This relation was determined from the "K-band disk central surface brightness" versus "disk scalelength" relation of DJ96 using only those galaxies with morphological type T lying within $0 \leq T \leq 6$. Similar results have been reported by Möllenhoff & Heidt (2001) and Graham (2001). Given the radial scalelength of the disk, it's scale-height z_s is calculated by $z_s = 0.25h_s$ (Pohlen et al. 2000). As for the geometry of the stellar population in the bulge, we assume that its scalelength, h_b, is equal to $0.14h_s$ (DJ96). The K-band absolute magnitude of the bulge, $M_{K,b}$, is determined by $M_{K,d}$ through the relation: $M_{K,b} = 16.5 + 1.6M_{K,d}$, which is the result of a linear fit to the DJ96 results (their Fig. 19) considering galaxies with $0 \leq T \leq 6$ only.

2.2. Dust spatial distribution and emission properties

The diffuse dust is distributed in another exponential disk with scalelength h_d and scaleheight z_d given by $h_d = 1.4h_s$ and $z_d = z_s/1.8$ (Xilouris et al. 1999). For the dust absorption and emission properties we are using the Milky-Way $R_V = 3.1$ model of Weingartner & Draine (2001).

Apart from the diffuse dust, a small but warm ammount of dust is expected to be found in HII regions. As in P00, a fraction F of the UV originating from the young stellar population is absorbed locally by the dust in these regions. In this study, we assume that this locally absorbed energy is re-emitted according to a spectrum template typical for star forming regions. The template is based on IRAS observations of HII regions in the Galaxy (Chini et al. 1986; Chan & Fich 1995) and in the Large Magellanic Cloud (Bell et al. 2002). In effect, this template is well approximated by thermal emission from dust with temperature 35 K.

To reduce the computational time of the model we did not take into account the stochastic heating of the diffuse dust. The dust emission due to stochastic heating affects the diffuse dust emission at 60 and 100 μm but the effect is small compared to the contibution from the localized dust emission from HII regions in these wavelengths. However, one expects that the inclusion of the stochastic heating would systematically yield more radiation from the diffuse dust at 60 and 100 μm. As a result less room would be left for dust emisson from the HII regions and the value of F would be lower.

2.3. Intrinsic luminosity of the old stellar population

Under these assumptions, the overall size and the bulge-to-disk ratio of each galaxy are essentially determined by $M_{K,d}$ and its morphological type. Furthermore, the disk and bulge magnitudes in the K band determine the intrinsic optical and near-infrared luminosity of each galaxy in the B, V, R, I, J and H bands through the relations: $B-V = 0.78$, $B-R = 1.23$, $B-I = 1.76$, $B-H = 3.30$ and $B-K = 3.59$. These are the weighted mean integrated colors for spiral galaxies with $0 \leq T \leq 6$, which we use for both the disk and bulge, since they are very similar (DJ96). Finally, we adopt $B-J = 2.69$ as given by Möllenhoff & Heidt (2001), based on their results from the surface photometry of 40 face-on disk galaxies. Note that the choice of the K-band luminosity as the basis for the determination of the intrinsic UV/optical radiation field was motivated by the fact that the light emitted in this band is the least affected by dust absorption when compared to the light emitted in other frequently observed bands, i.e. B through H. As a result, the observed K-band magnitudes can be considered as an accurate measure of the intrinsic galaxy luminosity, in this band.

2.4. The young stellar population

Finally, for the young stellar population we assume that it's spatial distribution can be described by an exponential disk with the same scalelength and scaleheight as that for the dust. The young stellar disk's luminosity is proportional to the SFR. Thus the luminosity of the young stellar population, L_λ, is expressed in terms of the SFR using the relations $SFR = 8.12 \times 10^{-28}\ L_\lambda$ [erg s^{-1} Hz^{-1}] at $\lambda = 912$ Å and $SFR = 1.4 \times 10^{-28}\ L_\lambda$ [erg s^{-1} Hz^{-1}] at $\lambda = 1200$ Å and $\lambda = 2800$ Å. These values were calculated with the PEGASE population

synthesis model of Fioc & Rocca-Volmerange (1997) assuming a Salpeter initial mass function with mass limits from 0.1 to 100 $M_{\odot}$, constant SFR and metalicity $Z = 0.02$. Note that different authors adopt slightly different conversion factors, depending on the parameters of the adopted population synthesis model (e.g. Bruzual & Charlot 2003). The intrinsic luminosity at the U band is attributed both to the young and the old stellar populations. Therefore, we have set it to the average of L_{2800} (which is assumed to originate only from the young stellar population) and L_B (which is assumed to originate only from the old stellar population). The ionizing UV (shortwards 912 Å) was neglegted since we assumed that it does not contribute significantly to dust heating

Details on the approximations we follow to solve the RTE can be found in Kylafis & Bahcall (1987). Since the geometry of the old and young stellar population and dust distribution, as well as the intrinsic old population luminosity in the optical and near-infrared bands are determined by the morphological type and by the disk and bulge K-band magnitudes, the theoretical SED is determined by introducing three free parameters only:

1. the central face-on optical depth in the V band τ_V, directly linked with the total dust mass of the galaxy, $M_{\rm d}$, through the relation
$$M_{\rm d} = \frac{4\pi\tau_V h_{\rm d}^2}{\sigma_V}, \quad (1)$$
where σ_V is the extinction cross section per unit mass for the dust in the V band;
2. the recent star formation rate SFR, which determines the intrinsic luminosity of the model galaxy in the UV (i.e. in the range from 912 to 3650 Å);
3. the fraction F of the locally absorbed UV, i.e. the fraction of the UV luminosity which is produced in the dense star-formation regions and is reprocessed locally, not being able to escape in the diffuse interstellar medium.

Having constructed a theoretical SED for a given galaxy, we can now compare it with its observed FIR spectrum, and thus determine values for SFR, dust mass and F.

3. The sample of galaxies

Our sample of galaxies with known FIR spectra is chosen from the sample of galaxies of DU00. These authors present SCUBA 850 μm observations for 104 galaxies chosen from the revised IRAS Bright Galaxy Sample (Soifer et al. 1989). The availability of 850 μm measurements for such a large number of galaxies is the most important property of the DU00 sample for our purposes, as measurements at the sub-mm waveband are crucial in order to constrain the FIR emission of a spiral galaxy. Some of these 104 galaxies have also been observed at 450 μm (Dunne et al. 2001).

First, we exclude galaxy pairs that were unresolved at the IRAS bands. Since K-band magnitudes are necessary for the determination of the geometrical characteristics of a galaxy and its optical and near infrared intrinsic luminosity, we used the NASA/IPAC Extragalactic Database (NED) to search for K-band measurements. The most recent 2MASS All-Sky Data Release provides total $K_{\rm S}$-band magnitudes ($M_{K_{\rm S}}$) for 60 galaxies in the DU00 sample. Note that, since the difference between the $K_{\rm S}$-band magnitudes and the K-band magnitudes of DJ96, who based their photometry on the standards of Elias et al. (1982), are typically of the order of ∼0.02 mag (see e.g. `www.astro.caltech.edu/jmc/2mass/v3/transformations/`), we will refer to the 2MASS magnitudes as simply the "K-band" magnitudes hereafter (i.e. we assume that $M_K = M_{K_{\rm S}}$). We found M_K magnitudes for 8 more galaxies in Spignolio et al. (1995). Apart from the availability of M_K, the morphological type of each galaxy is also important in determining its geometrical characteristics, as explained in the previous section. For this reason we used the Third Reference Catalog of Bright Galaxies (RC3; de Vaucouleurs et al. 1991) in order to search for the T value of each galaxy in the DU00 list of objects.

Our final sample consists of those 68 galaxies in the DU00 list 2000 with known M_K and morphological type $0 \leq T \leq 6$. Table 1 lists their basic properties like distance (in Mpc; Col. 2) as taken from DU00, and $M_{K,\rm d}$ (Col. 3). The following 3 columns list the 60 and 100 μm IRAS measurements (Soifer et al. 1989) and the SCUBA 850 μm measurements of DU00. Column 7 lists the logarithm of the total gas mass, $M_{\rm g}$. In the cases where both atomic and molecular hydrogen masses are available, $M_{\rm g}$ is their sum. In the cases where either the atomic or the molecular is available we presumed that the total mass is twice as much. The data for the gas masses are taken from DU00, and are based on measurements of Sanders & Mirabel (1985), Sanders et al. (1986, 1991), Huchtmeier & Richter (1989), Bottinelli et al. (1990), Young et al. (1995), Casoli et al. (1996), Chini et al. (1996), Maiolino et al. (1997), Solomon et al. (1997), Lavezzi & Dickey (1998) and Theureau et al. (1998). Note that, although there are 68 galaxies in the sample, Table 1 has 62 entries as we can not fit well the FIR SED of 6 galaxies (see Sect. 4). As a result, we can not calculate their SFR, dust mass and F, and for that reason these galaxies do not appear in Table 1.

In Fig. 1 we plot $M_{K,\rm d}$ as a function of T for the galaxies in our sample. In most cases $-25 \leq M_{K,\rm d} \leq -23$, with the average $M_{K,\rm d}$ value being equal to −23.9. There is no clear trend between $M_{K,\rm d}$ and T. If we compare this figure with Fig. 6 in DJ96, we see that, for all T, the $M_{K,\rm d}$ magnitudes of the galaxies in the present sample are brighter than the magnitudes of the galaxies in the DJ96 sample which included all T. Since DJ96 uses a statistically complete sample of spiral galaxies, we conclude that the galaxies in our sample are more luminous than the average, typical spirals, irrespective of their morphological type.

4. Fitting the model to the data

The model SED is fitted to each set of FIR measurements by first fixing the galaxy disk and bulge absolute magnitude in the K band to the observed values, hence determining the geometrical parameters of the galaxy and the luminosity of the old stellar population, as explained in Sect. 2. Then the three free parameters of the model (SFR, dust mass and F) are varied in order to minimize the sum of the squares of the differences

Table 1. Data and model parameters of the galaxies in our sample. Details in Sect. 3.

NAME	Distance Mpc	$M_{K,\mathrm{d}}$	log L_{60} W/Hz/sr	log L_{100} W/Hz/sr	log L_{850} W/Hz/sr	log M_{g} $M_{\odot}$	log M_d $M_{\odot}$	log SFR $M_{\odot}$/yr	F	A_{1800}
NGC 23	61.0	−24.82	23.49	23.72	21.70	10.22	7.96	1.34	0.53	1.12
UGC 556	62.0	−23.52	23.29	23.56	21.45	9.93	7.65	1.25	0.39	0.90
NGC 470	32.0	−23.56	22.83	23.06	21.31	9.78	7.69	0.58	0.69	1.62
UGC 903	34.0	−23.14	22.93	23.19	21.28	9.82	7.57	0.83	0.49	1.12
NGC 520	30.0	−23.86	23.44	23.61	21.45	10.13	7.65	1.24	0.65	1.45
NGC 697	42.0	−24.44	22.96	23.43	21.56	10.67	7.84	1.14	0.16	0.50
NGC 772	33.0	−25.13	22.84	23.39	21.47	10.57	7.73	1.26	0.03	0.21
NGC 877	52.0	−24.52	23.48	23.78	21.93	10.48	8.24	1.39	0.47	1.11
NGC 958	77.0	−25.69	23.51	23.92	22.16	10.74	8.50	1.47	0.29	0.72
NGC 992	55.0	−23.76	23.50	23.66	21.63	10.27	7.91	1.24	0.76	2.00
NGC 1134	49.0	−24.45	23.31	23.56	21.74	10.58	8.08	1.12	0.58	1.32
UGC 2403	55.0	−23.68	23.34	23.54	21.51	10.14	7.77	1.15	0.63	1.46
UGC 2982	71.0	−24.26	23.62	23.92	21.92	10.46	8.17	1.57	0.41	1.00
NGC 1667	61.0	−24.80	23.34	23.76	21.76	10.18	7.98	1.50	0.16	0.49
NGC 2782	34.0	−23.66	23.03	23.21	21.42	9.81	7.81	0.72	0.81	2.23
NGC 2856	35.0	−23.30	22.86	23.08	21.02	9.45	7.25	0.74	0.50	1.01
NGC 2966	27.0	−22.41	22.61	22.79	20.98	9.44	7.36	0.34	0.77	2.04
NGC 2990	41.0	−22.88	22.95	23.21	21.25	9.99	7.51	0.86	0.47	1.11
IC 563	81.0	−23.61	23.26	23.56	21.81	10.10	8.14	1.22	0.44	1.10
IC 564	80.0	−24.31	23.18	23.60	21.88	10.10	8.22	1.24	0.29	0.82
NGC 3110	67.0	−24.41	23.70	24.00	21.91	10.64	8.10	1.68	0.36	0.89
NGC 3221	55.0	−24.62	23.33	23.75	21.86	10.49	8.13	1.42	0.23	0.66
NGC 3367	40.0	−24.09	22.98	23.29	21.31	10.07	7.57	0.98	0.33	0.69
NGC 3583	28.0	−23.72	22.74	23.18	21.15	9.90	7.37	0.99	0.12	0.38
MCG+00-29-023	102.0	−24.42	23.73	23.94	21.92	10.68	8.17	1.56	0.60	1.41
UGC 6436	137.0	−24.43	24.00	24.24	22.27	10.44	8.54	1.90	0.50	1.22
NGC 3994	41.0	−23.23	22.91	23.22	21.24	10.05	7.48	0.91	0.35	0.80
NGC 4045	26.0	−23.22	22.63	22.95	20.97	9.43	7.22	0.67	0.32	0.67
NGC 4273	32.0	−23.30	23.00	23.30	21.49	9.94	7.81	0.94	0.45	1.09
NGC 4433	40.0	−23.39	23.33	23.53	21.52	10.06	7.79	1.15	0.63	1.50
NGC 4793	33.0	−23.57	23.11	23.46	21.43	10.04	7.65	1.18	0.26	0.68
NGC 5020	45.0	−24.03	23.01	23.28	21.59	10.37	7.98	0.79	0.63	1.49
NGC 5104	74.0	−24.41	23.55	23.83	21.68	10.13	7.85	1.54	0.33	0.75
NGC 5256	111.0	−25.21	23.93	24.09	21.99	10.66	8.24	1.67	0.74	1.77
UGC 8739	67.0	−24.81	23.40	23.79	21.90	10.42	8.18	1.45	0.28	0.72
NGC 5371	34.0	−24.81	22.77	23.30	21.18	10.35	7.39	1.36	0.01	0.16
NGC 5426	35.0	−23.12	22.55	22.99	21.52	10.72	7.92	0.62	0.32	0.88
NGC 5427	36.0	−24.03	22.94	23.31	21.52	10.38	7.83	0.95	0.33	0.78
NGC 5600	31.0	−22.95	22.69	23.02	21.01	9.35	7.24	0.73	0.30	0.69
NGC 5653	47.0	−24.66	23.34	23.67	21.64	9.87	7.87	1.37	0.30	0.68
NGC 5665	30.0	−22.82	22.71	22.99	21.12	9.27	7.42	0.62	0.48	1.08
NGC 5676	28.0	−24.15	22.96	23.35	21.56	10.18	7.88	0.99	0.30	0.73
NGC 5713	25.0	−23.53	23.10	23.34	21.34	10.11	7.60	0.99	0.49	1.08
NGC 5792	26.0	−24.19	22.77	23.06	21.38	10.31	7.78	0.45	0.67	1.53
NGC 5900	33.0	−23.07	22.89	23.25	21.28	9.93	7.52	0.94	0.30	0.76
NGC 5936	53.0	−24.01	23.36	23.66	21.61	9.95	7.84	1.34	0.37	0.85
NGC 5937	37.0	−23.66	23.12	23.42	21.50	9.51	7.78	1.07	0.41	0.96
NGC 5962	26.0	−23.42	22.77	23.13	21.31	9.77	7.62	0.78	0.34	0.80
NGC 5990	51.0	−24.40	23.36	23.59	21.44	9.53	7.62	1.29	0.43	0.85
NGC 6052	63.0	−23.30	23.38	23.58	21.55	10.18	7.81	1.21	0.62	1.49
NGC 6181	32.0	−23.72	22.95	23.30	21.34	10.07	7.59	1.00	0.29	0.68
NGC 7448	29.0	−23.19	22.83	23.14	21.19	9.83	7.46	0.82	0.37	0.83
ZW 453.062	100.0	−24.24	23.83	24.00	21.82	9.76	8.00	1.62	0.66	1.56
NGC 7541	36.0	−24.25	23.39	23.69	21.71	10.39	7.96	1.35	0.40	0.92
ZW 475.056	109.0	−24.60	24.00	24.12	21.94	10.21	8.16	1.71	0.83	2.29
NGC 7591	66.0	−24.31	23.51	23.75	21.75	10.42	8.01	1.38	0.53	1.18
NGC 7674	116.0	−25.25	23.83	24.00	22.14	10.79	8.52	1.50	0.83	2.39
NGC 7678	47.0	−24.06	23.16	23.48	21.60	10.00	7.89	1.13	0.38	0.89
NGC 7771	57.0	−25.16	23.80	24.06	22.06	10.38	8.32	1.69	0.47	1.05
UGC 1351	61.0	−24.09	23.33	23.61	21.69	10.09	7.98	1.24	0.46	1.08
UGC 1451	66.0	−24.17	23.44	23.70	21.64	9.93	7.87	1.36	0.44	0.98
NGC 3094	32.0	−22.81	23.05	23.17	21.17	9.65	7.52	0.72	0.91	3.07

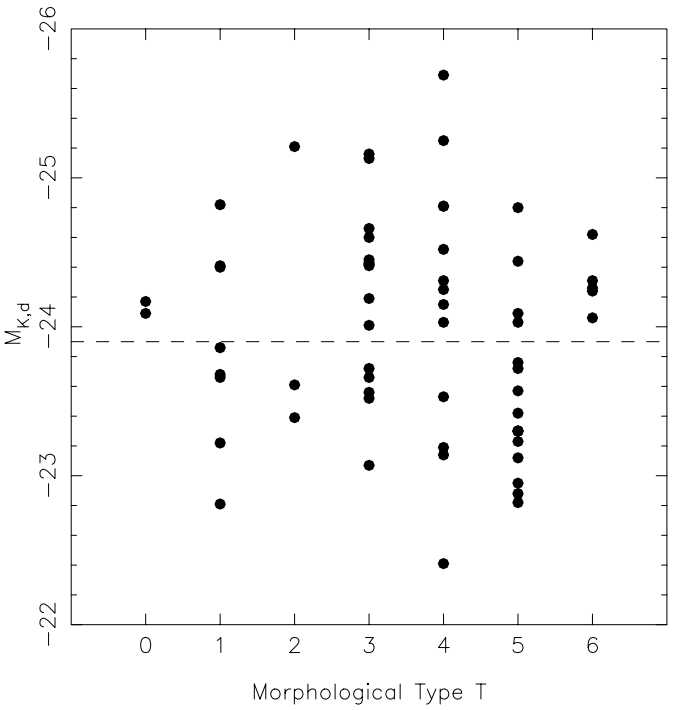

Fig. 1. The disk K-band magnitudes of the galaxies in our sample plotted as a function of galaxy morphological type, T. The dashed line indicates the average $M_{K,\mathrm{d}}$ value for the whole sample.

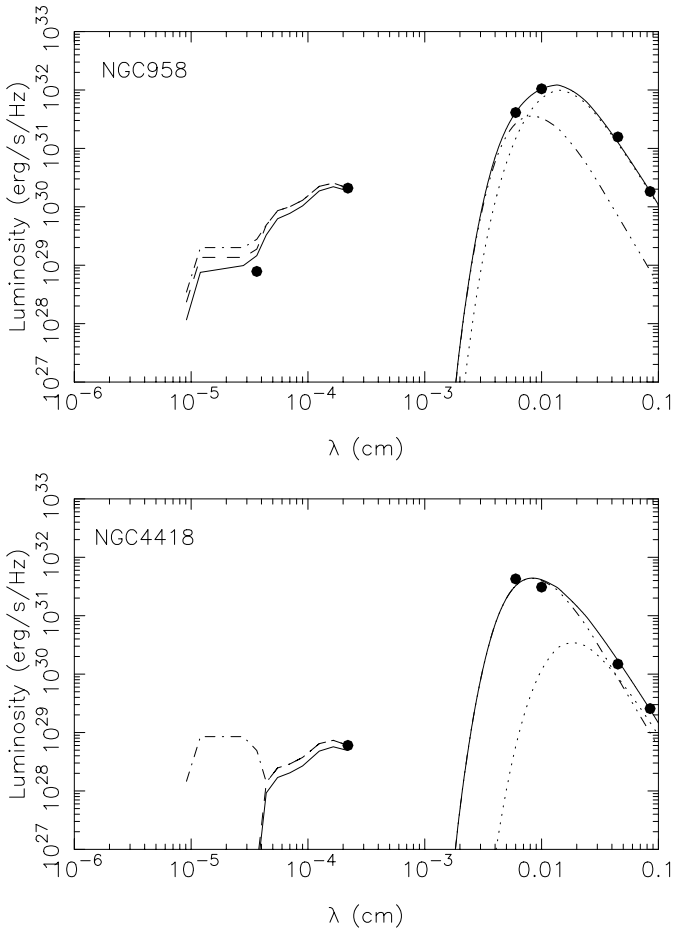

Fig. 2. Examples of a good (*upper plot*) and a bad (*bottom plot*) model fit to the FIR spectrum of a galaxy. The three lines in the UV-optical bands represent the intrinsic luminosity (dot-dashed line), the luminosity after subtracting the locally absorbed radiation (dashed line), the luminosity after taking into account the absorption, both locally and from the diffuse dust (solid line). The three-dot-dashed, dotted, and solid lines in the FIR band represent the emission from dust in the HII regions, the emission spectrum of the diffuse dust and the total FIR emission, respectively.

between the logarithms of the model and the observed luminosity at 60, 100 and 850 μm (L_{60}, L_{100}, and L_{850} respectively). The minimization is done using the Steve Moshier C translation of the public domain Levenberg-Marquardt solver of the Argonne National Laboratories MINPACK mathematical library available at `www.netlib.org`.

Our model is able to fit very well the observed FIR spectrum of most galaxies. As an example, we show in the upper panel of Fig. 2 the model SED (solid line) and the observed FIR spectrum of the galaxy NGC 958. Filled circles in the right hand part of the plot show the observed L_{60}, L_{100}, L_{450} and L_{850} measurements. The other two points in the UV and near-IR part of the spectrum show the observed U- and K-band luminosities. The dot-dashed line in the left hand part of the plot represents the intrinsic UV and optical SED. The dashed line represents the UV SED after the UV absorption in the HII regions has been subtracted. The solid line represents the UV and optical SED after absorption in the diffuse dust of the galaxy has also been taken into account. In the FIR part of the spectrum, the three-dot-dashed line shows the emitted spectrum of the HII regions, and the dotted line shows the emitted spectrum of the diffuse dust. Finally, the solid line represents the sum of these two components (i.e. the total FIR emission). This figure shows clearly that the model FIR SED fits very well the observed FIR spectrum. The predicted UV flux agrees well with the observed U flux as well, as their ratio is smaller than two.

However, we can not fit well the observed FIR spectrum of six galaxies in our sample, namely, MCG+02-04-025, NGC 1614, NGC 4418, IC 860, NGC 7714 and MRK 331.

The ratio L_{60}/L_{100} in these galaxies is higher than 0.8. This is the maximum flux ratio value that can be explained by the fixed template we use for the dust emission from HII regions. This is the main reason for the failure of the model to provide a good fit to the FIR spectra of these galaxies. In the bottom panel of Fig. 2, we show a plot of the observed FIR spectrum and the best fitting model SED in the case of NGC 4418. The lines drawn in this plot have the same meaning as the lines shown in the upper panel of the same figure. Although the model fits well the SCUBA measurements, it fails to fit well the IRAS fluxes. Comparison of the observed FIR SEDs between the two galaxies shown in Fig. 2 reveals clearly the difference in the IRAS colors of NGC 958 and NGC 4418, with the second being significantly "warmer". In all cases where we cannot fit well the FIR SED, the best fitting F values are almost equal to 1, which in effect implies that almost all the FIR emission in these galaxies is produced in HII regions. Although this may well be the case, the bad quality of the model fitting to their FIR spectra prevents us from drawing conclusive results in these cases. While we could get a better model fit to the

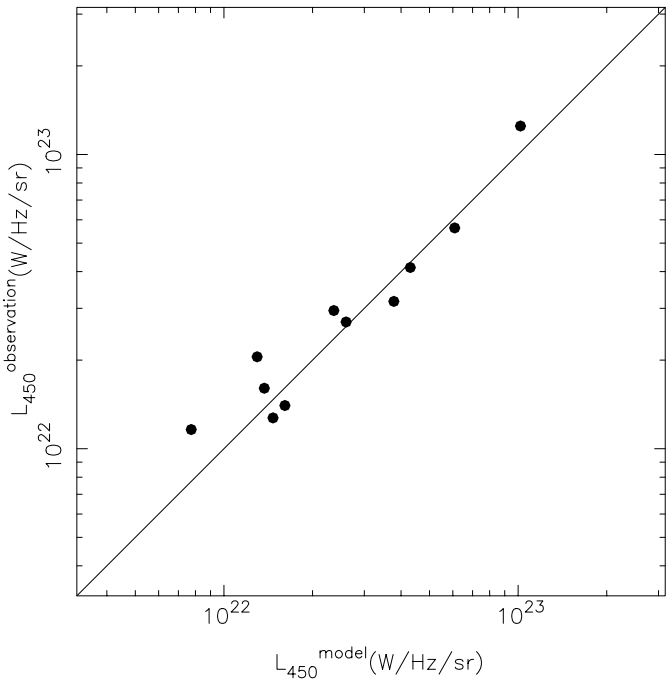

Fig. 3. Comparison of the model predicted and the observed luminosity at 450 μm. The solid line shows the $L_{450}^{\rm observed} = L_{450}^{\rm model}$ relation, and *not* the best fitting model to the data. It is plotted in order to guide the eye, and to demonstrate clearly the good agreement between the model predicted and observed L_{450}.

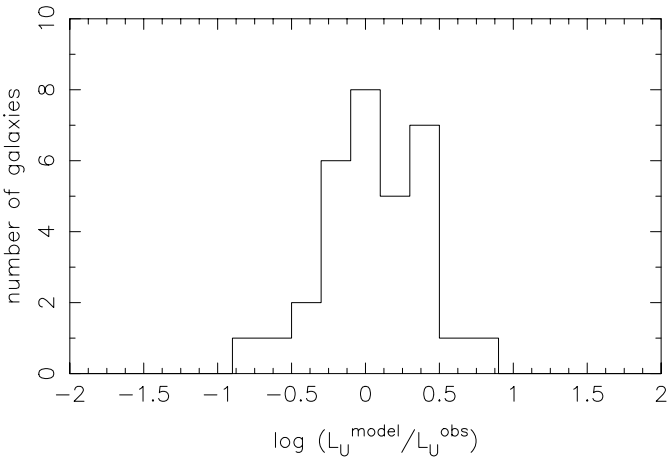

Fig. 4. Comparison of the model predicted and the observed UV luminosity for the galaxies of our sample with published photometry in the U band.

FIR spectra of these six galaxies using a higher temperature for the dust emission in the HII regions, this would lead to the adoption of an extra free parameter to characterize the emission properties of the HII regions. Since a detailed description of the properties of HII regions in spiral galaxies does not lie within the scope of this paper we decided to exclude these galaxies from the discussion hereafter. As a result, we end up with 62 galaxies for which we have managed to fit well their FIR spectra and hence calculate the dust mass, the SFR and the F for them. The best model fitting values are listed in Table 1, Cols. 8, 9, and 10 respectively.

Finally, although there are SCUBA 450 μm measurements for some of the galaxies in our sample (Dunne et al. 2001), we do not take them into account during the model fitting of their FIR spectrum. Having found though the best fitting model parameters for each galaxy, we can now compare the model predicted and observed flux values at 450 μm. Figure 3 shows this comparison plot. The model predicted flux values agree very well with the observed values. This is an important result, as this excellent agreement justifies the dust emission properties we have used and strongly suggests that the dust emissivity index β is very close to $\beta = 2$, as argued by Weingartner & Draine (2001).

5. Results

5.1. SFR estimates

The best fitting SFR values of the galaxies in our sample range roughly from 2 $M_\odot\,{\rm yr}^{-1}$ to 80 $M_\odot\,{\rm yr}^{-1}$, with an average value of 19 $M_\odot\,{\rm yr}^{-1}$. These values lie between the SFR estimates for late type, gas-rich spirals and optically-selected starburst galaxies (Kennicutt 1998b). In order to investigate whether the model computed SFRs are realistic or not, we perform the following test. Using the RC3 catalog, we find that 32 out of the 62 galaxies in the sample have known U-band magnitudes. Since the model intrinsic UV emission is uniquely determined by the adopted SFR value, the comparison between the model predicted and the observed U-band luminosity can give us direct information on the accuracy of the model resulting SFR. Figure 4 shows a plot of the statistics for the ratio of the model ($L_U^{\rm model}$) over the observed luminosity ($L_U^{\rm obs}$) in the U-band. The average $L_U^{\rm model}/L_U^{\rm obs}$ value of 1.4 implies a good agreement between the model and the observed luminosities. The scatter of the $L_U^{\rm model}/L_U^{\rm obs}$ values around unity is expected because a) the true radii of the galaxies are expected to "scatter" around the adopted values (which were not measured directly but were based on the observed $M_{K,\rm d}$ values), b) the temperature of the dust in the HII regions in the individual galaxies is naturally expected to "scatter" around the assumed value of 35 K, and c) $L_U^{\rm model}$ is the integrated intensity for the total 4π solid angle around the galaxy, without taking into account the inclination of these galaxies. We conclude that the close agreement between $L_U^{\rm model}$ and $L_U^{\rm obs}$ implies that the model derived SFR values are close (within a factor of ∼2) to the intrinsic values for each galaxy in the sample. This fact, together with the fact that the model SEDs agree very well with the observed FIR spectra give us confidence that the model derived dust mass and F values should also represent correctly the respective intrinsic values for the galaxies under study.

The large range in SFR values that we derive reflects the corresponding large range of absolute luminosities in the galaxies. Indeed, we find a positive correlation between SFR and $M_{K,\rm d}$ in the sense that more luminous galaxies do show a larger SFR (in absolute units). However, when we divide the SFR values by the K-band, disk luminosity, $L_{K,\rm d}$, we find that the normalized SFR values decrease with increasing luminosity, according to the relation $SFR_{\rm norm} \propto L_{K,\rm d}^{-0.15}$. This relation implies an anticorrelation between SFR per unit luminosity and

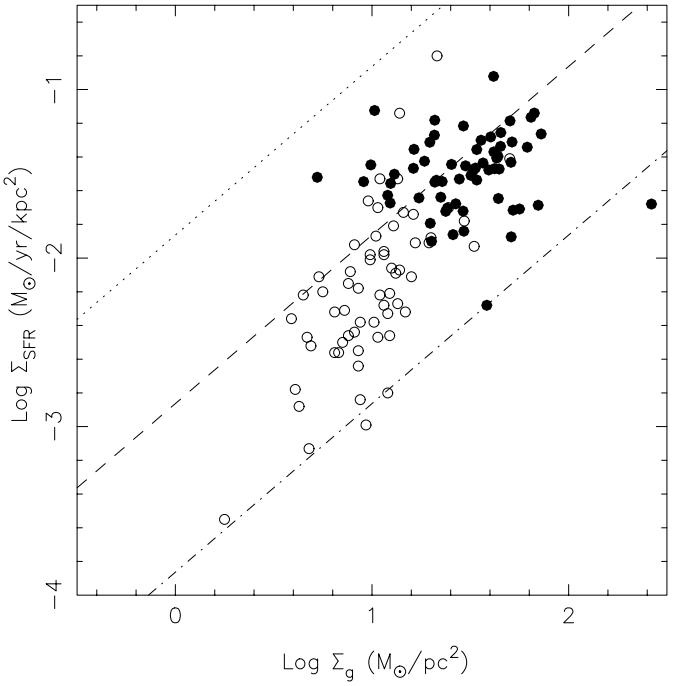

Fig. 5. Star-formation-rate surface density as a function of gas surface density for the galaxies in our sample (solid circles). Open circles show data from 61 normal spiral galaxies by Kennicutt (1998a). The dotted, dashed and dot-dashed lines correspond to star formation efficiencies of 100%, 10%, and 1% in 10^8 yr.

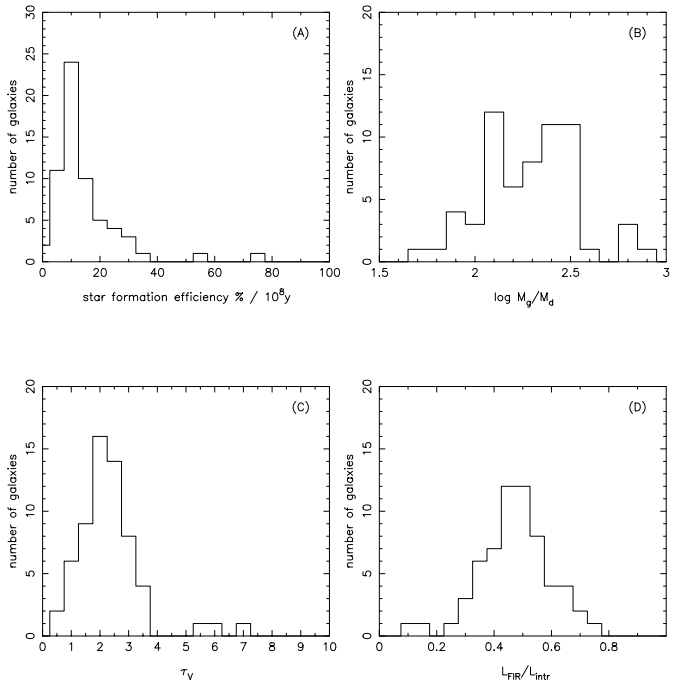

Fig. 6. Sample distribution plots of the following model derived parameters: Star formation efficiency for a time scale of 10^8 years (Panel **A**), gas-to-dust mass ratio (Panel **B**), central face-on optical depth in the V band (Panel **C**), FIR to total intrinsic luminosity ratio (Panel **D**).

galaxy mass (as parametrized by $L_{K,\mathrm{d}}$); more massive galaxies appear to have a smaller SFR per unit mass. This is qualitatively similar to the results from previous works. For example, Gavazzi et al. (1996) also find an anticorrelation between star formation rate (normalized to the H-band luminosity) and the mass of the galaxy (as parametrized by the H-band luminosity).

We also investigate the relation of SFR with the gas content of the galaxies. For this reason we divide the SFR and gas mass of each galaxy by the surface of the disk, assuming a truncation radius of 3 disk scalelengths (Pohlen et al. 2000). Figure 5 shows the plot of SFR surface density as a function of gas surface density (solid circles). In the same figure we also plot the SFR and gas surface density measurements of 61 normal spiral galaxies from Kennicutt (1998a). The galaxies of the present sample have larger average gas and SFR surface densities, when compared to the respective values of the sample of normal galaxies. This is not unexpected, as they are IRAS bright galaxies, so one expects them to have both larger SFR and gas densities when compared to normal galaxies. Nevertheless, the relation between SFR surface density and gas surface density is in agreement with the same relation as defined by the data of the normal galaxies alone. Figure 5 also shows the constant, disk-averaged 1%, 10%, and 100% star formation efficiency per 10^8 years (dot-dashed, dashed, and dotted lines respectively). The star formation efficiency is defined as the percentage of the gas mass that is converted to stars assuming constant SFR for a period of 10^8 years. The distribution of the star-formation efficiency values is shown in panel (A) of Fig. 6. For almost all galaxies, the star formation efficiency lies between 5% and 30%. The average value for the galaxies in our sample is 14%, slightly larger than the respective value of the normal spiral galaxies, but close to the typical value for gas rich spirals.

5.2. The dust mass estimates

In most studies, the dust emission in spiral galaxies is modeled with one or more gray-body components of constant temperature. Usually a "warm" and a "cold" component are assumed, their combined spectra are fitted to the observed FIR spectra, and as a result the dust masses and the temperatures of the components are derived (e.g. Alton et al. 1998, 2001; Haas et al. 1998; Davies et al. 1999; Lisenfeld et al. 2000, 2002; Trewhella et al. 2000; Irwin et al. 2001; Popescu et al. 2002; Bendo et al. 2003; Böttner et al. 2003; Dupac et al. 2003; Hippelein et al. 2003).

While our model also assumes two components, they are introduced in a natural way and they correspond to physically distinct dust components within the galaxy. The temperature of the "warm" component is kept fixed at 35 K, according to the results from FIR observations of dense, HII regions, but the temperature of the "cold" component is not fixed. In fact, this component does not even have the same temperature throughout its volume. Instead, its temperature varies with the distance from the galaxy's center, and is computed through the solution of the radiative transfer equation. As a result, our dust mass calculations are less affected by assumptions about the dust temperature of the warm component and the wavelength dependence of the dust emissivity.

The dust masses that we derive range from $M_{\rm d} \sim 10^7\ M_\odot$ to $M_{\rm d} \sim 3\times10^8\ M_\odot$ and lie within the accepted range for spiral galaxies. The large range of dust-mass values reflect again the large range of absolute magnitudes. Knowing the gas mass as well, we can now compute the gas-to-dust mass ratio ($M_{\rm g}/M_{\rm d}$) for each galaxy in the sample. The distribution of the $M_{\rm g}/M_{\rm d}$ values is shown in panel (B) of Fig. 6. The value of this ratio lies within 100 and 300 for most of the galaxies, while its mean value is 250, in excellent agreement with the generally accepted value for our galaxy. In the past, gas-to-dust ratios of the order of ∼5−10 times higher than the Galactic value were found for bright IRAS galaxies (Devereux & Young 1990; Sanders et al. 1991). Our results demonstrate that when the full band FIR spectrum is taken into account and modeled with a realistic physical model, then the gas-to-dust mass ratio for bright IRAS galaxies is similar to the Galactic value.

Apart from the dust mass, we can also calculate the central face-on optical depth, using Eq. (1). Panel (C) in Fig. 6 shows the distribution of the central face-on optical depth at the V band, τ_V. We find no correlation between τ_V and size of the galaxy (as parametrized with the use of $M_{K,\rm d}$ values). Most of the galaxies exhibit a central face-on optical depth between 1 and 4, while the mean value is 2.3. In other words, we find that these bright IRAS galaxies tend to have an average central face-on optical depth somewhat larger than unity.

5.3. The F estimates

The value of the fraction F of the locally absorbed UV, covers the full range from almost zero to almost one for the galaxies in our sample. In most cases though this value lies between 0.3 and 0.6. We find no correlation between F and either SFR or $M_{K,\rm d}$. However, we do find a strong correlation between F and the ratio of the luminosity at 60 μm over the luminosity at 100 μm: $F \propto (L_{60}/L_{100})^{2.3}$. In other words, we find that warmer FIR spectra (in terms of the 60 over 100 μm flux ratios) exhibit higher percentage of local absorption of UV in star forming regions.

Finally, we also compute the ratio of the FIR luminosity over the total intrinsic UV/optical/NIR luminosity, $L_{\rm FIR}/L_{\rm intr}$. The distribution of the ratio values is shown in panel (D) of Fig. 6. The values cover the range from 0.4 to 0.6, with the mean value being 0.54. Popescu & Tuffs (2002) studied 28 Virgo cluster galaxies ranging from S0 to Sm and found $L_{\rm FIR}/L_{\rm intr}$ values between 0.15 and 0.5. Our sample seems to be complementary to theirs in the sense that our sample consists of large, gas rich spirals that are strong IRAS sources, while their sample consists of normal galaxies. Yet we find no correlation of $L_{\rm FIR}/L_{\rm intr}$ with morphological type as they do.

We also find no correlation between $L_{\rm FIR}/L_{\rm intr}$ and either SFR or $M_{K,\rm d}$. However, we do find a significant correlation between $L_{\rm FIR}/L_{\rm intr}$ and F, in the sense that as F increases, then $L_{\rm FIR}/L_{\rm intr}$ increases as well, following the relation $L_{\rm FIR}/L_{\rm intr} = 0.25 + 0.5F$. Perhaps then, the difference in the average $L_{\rm FIR}/L_{\rm intr}$ value between normal spirals and the bright IRAS galaxies of the present sample may simply reflect the difference in their average F values.

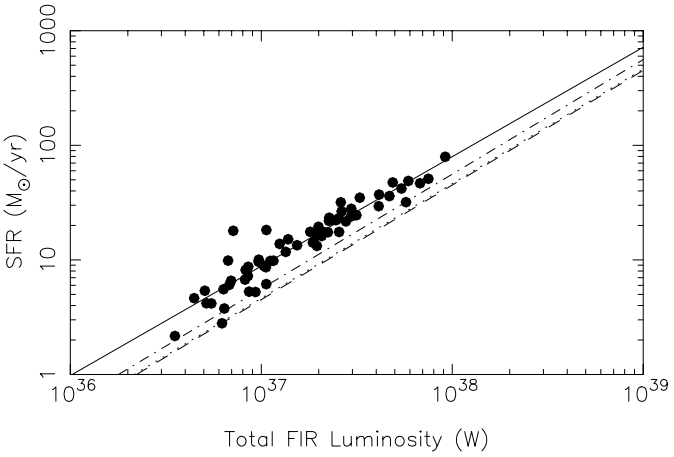

Fig. 7. Star formation rate as a function of Total FIR luminosity. The solid line is a best linear fit (in log–log space). The dashed line is drawn according to the $L_{\rm FIR}$−SFR relation of Kennicutt (1998b) for starburst galaxies. The dot-dashed line represents the same relation as calibrated by Buat & Xu (1996). Finally the dotted line represents the calibration of Panuzzo et al. (2003).

The fraction of the locally absorbed UV is directly linked with the overall attenuation in the UV band (due to both locall absorption and absorption from the diffuse dust). To enable the comparison with other works we have also calculated the extinction of each galaxy at 1800 Å. The calculated values are given in the last locumn of Table 1. The extinction at 1800 Å ranges from 0.2 to 3.1 mag.

6. FIR diagnostic relations

Since our model provides a good fit to the observed FIR spectra of the galaxies in the sample, we now proceed to investigate if we can find significant correlations between their observed FIR properties and the SFR and dust-mass values. To this aim, we use the results listed in Table 1 and correlate the model derived parameter values with various observed FIR quantities. The set of "observed quantities" vs. "model parameters", which provide the most significant correlations (or alternatively relations with the least possible scatter in then) can then be used as a basis to derive diagnostic relations between SFR, dust mass and FIR observations.

6.1. SFR diagnostics

We find that the SFR is well correlated with the total FIR luminosity, $L_{\rm FIR}$ (computed using the model FIR spectrum over the wavelength range 10−2000 μm), and L_{60}, L_{100}, L_{850}. The best correlations, i.e. the ones with the least scatter, are found between SFR and $L_{\rm FIR}$ and between SFR and L_{100} (shown as solid lines in Figs. 7 and 8, respectively). The best linear-model fit to the SFR vs. $L_{\rm FIR}$ plot (in log–log space) yields the following relation:

$$\log\left(\frac{SFR}{M_\odot\ {\rm yr}^{-1}}\right) = -34.4 + 0.95\log\left(\frac{L_{\rm FIR}}{W}\right). \quad (2)$$

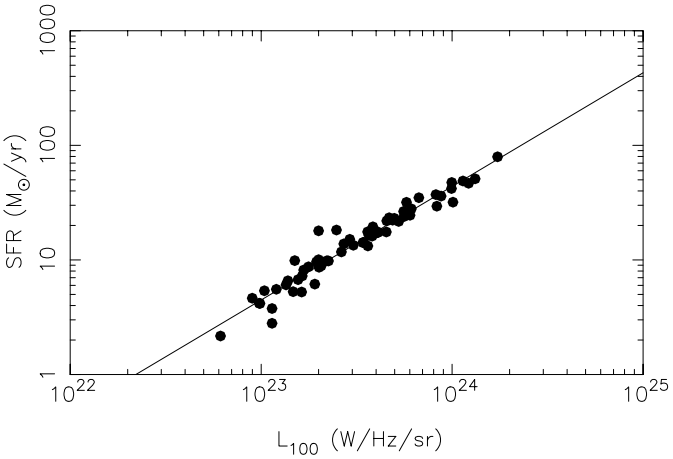

Fig. 8. Star formation rate ploted as a function of L_{100}. The solid line is a best linear fit (in log–log space).

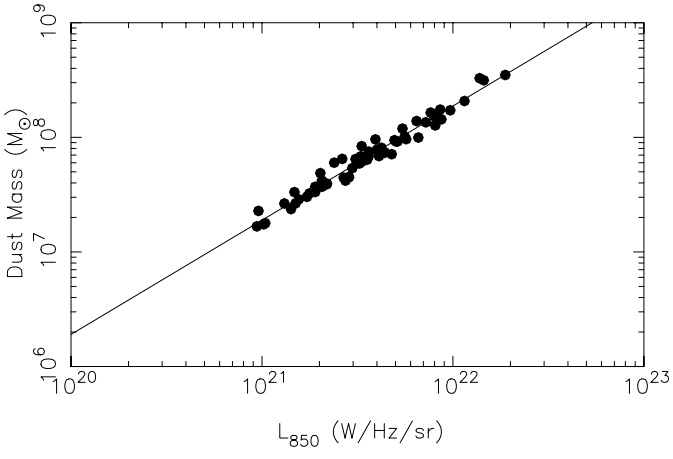

Fig. 9. Dust mass as a function of Luminosity at 850 μm. The solid line shows the best linear fit (in log–log space).

The relation given by Buat & Xu (1996) is drawn also in Fig. 7 as a dot-dashed line[2]. These authors quote a margin of error of the order of 2. On average, the scatter in our case is smaller, as can be seen from Fig. 7. However, as Fig. 4 shows, we do expect our SFRs to be uncertain by a factor of 2, so the uncertainty of the SFR of Eq. (2) should be of that order. The dotted line represents the relation between FIR and SFR from Panuzzo et al. (2003). The large disagreement can be attributed to the higher attenuation of their model which causes the absorption of more stellar radiation. Similar SFR$-L_{\rm FIR}$ relations have been introduced in the past for starburst galaxies. The relation with the calibration of Kennicutt (1998b) is drawn in Fig. 7 as a dashed line. Bell (2003) presents a similar result. It is clear that, in the case of our sample, a given FIR luminosity yields roughly twice as much SFR as starburst galaxies due to the reduced percentage of starlight which is absorbed and re-emitted in the FIR in the latest.

The very good correlation between SFR and L_{100} shown in Fig. 8 is not surprising. The maximum of the FIR emission lies between 100 and 200 μm and therefor L_{100} traces well the total FIR emission, which in turn depends on SFR. The best linear model fit to the SFR vs. L_{100} plot (in log–log space) yields the following relation:

$$\log\left(\frac{SFR}{M_\odot\,\mathrm{yr}^{-1}}\right) = -22.1 + 0.99\log\left(\frac{L_{100}}{W\,\mathrm{sr}^{-1}\,\mathrm{Hz}^{-1}}\right). \quad (3)$$

Note that this relation may be more useful in practice than the relation defined by Eq. (2), as L_{100} is a directly measured quantity, while $L_{\rm FIR}$ in Eq. (2) is derived from the model FIR SED. In practice, empirical methods will introduce an extra component of uncertainty in the estimation of $L_{\rm FIR}$ and hence SFR.

It is not clear whether Eqs. (2) and (3) can be used to estimate the SFR for *all* spiral galaxies with morphological type index $0 \le T \le 6$, similar to the galaxies studied in this work. This depends on whether the contribution of the old stellar population to dust heating changes with galaxy luminosity or not. The average value of the ratio of dust heating caused by the old and the young stellar population is 0.2 for the galaxies in our sample, indicating, that 80% of the dust heating originates in the young stellar population. We find no correlation between this ratio and M_K, i.e. the galaxy's luminosity. However, the galaxies studied in this work have M_K magnitudes which are brighter than these of the typical spiral galaxies. We caution then that Eqs. (2) and (3) may not be applicable to less luminous galaxies, i.e. galaxies with $M_K > -23$. This issue will be resolved in the future, when SCUBA observations of a large number of spiral galaxies with magnitudes fainter than, say, $M_K = -23$ will be available. In this case, we will be able to study their FIR spectrum in a similar fashion, and investigate whether Eqs. (2) and (3) can be applied to them as well.

6.2. Dust mass diagnostics

We find that $M_{\rm d}$ is well correlated with L_{850}. Figure 9 shows the diffuse dust mass plotted as a function of L_{850}. This figure shows clearly the excellent correlation between $M_{\rm d}$ and L_{850}. In fact, the relation between these two quantities is linear although we do not consider a single value for the dust temperature of the "cold" component (in which case the relationship between $M_{\rm d}$ and L_{850} is linear by identity). The best-fitting linear model (in log–log space) yields the relation,

$$\log\left(\frac{M_{\rm d}}{M_\odot}\right) = -13.6 + 0.997 \times \left(\frac{L_{850}}{W\,\mathrm{sr}^{-1}\,\mathrm{Hz}^{-1}}\right). \quad (4)$$

While this relation can be used to derive the dust mass from the 850 μm flux one has to keep in mind that the calibration depends on the adopted cross section per unit mass σ_{850} of the dust at the 850 μm. The use of a larger value for σ_{850} will result in a reduced $M_{\rm d}$ value and vice versa. In this study we have implicity used the value of 0.505 cm^2 gr^{-1}, as suggested by the model of Weingartner & Draine (2001). However, other theoretical models suggest values that go up to 3 cm^2 gr^{-1} (e.g. Mathis & Whiffen 1989; Ossenkopf & Henning 1994). Furthermore, there are observational attempts to measure σ_{850} mainly by comparing the dust attenuation in the optical band with the emission at 850 μm. Alton et al. (2000) cite a value of

[2] In their paper, Buat & Xu (1996) used the FIR from 40 to 120 μm. In our spectra roughly 70% of the total FIR emission lies in this range. To compare our result with theirs we have corrected their relation accordingly.

1.29 cm^2 gr^{-1} (for NGC 891), Bianchi et al. (1999) based on data from the Galaxy argue for 0.37 cm^2 gr^{-1}, while in a subsequent work based on Barnard 68, Bianchi et al. (2003) find a higher value of 1.5 cm^2 gr^{-1}. Finally, James et al. (2002) use a different method based on metalicity and find σ_{850} equal to 0.7 cm^2 gr^{-1}.

7. Summary

We use the realistic physical model of P00 to study the FIR spectrum of 62 bright IRAS galaxies. The model takes into account the 3D spatial distributions of both the old and young stellar populations, and the geometry of the dust. The intrinsic optical and NIR SEDs of each galaxy are determined by the observed K-band magnitude, while the UV SED is proportional to the star-formation rate through the use of the population synthesis model of Fioc & Rocca-Volmerange (1997). By solving the radiative transfer equation, we derive the FIR SED which we then fit to the observed FIR spectra of each galaxy in order to derive values for the SFR, the dust mass and the fraction, F, of the UV radiation which is locally absorbed in the HII regions.

The sample of galaxies studied in this work consists of late-type spiral galaxies ($0 \leq T \leq 6$) whose M_K magnitudes are brighter than the average K-band magnitudes of normal spiral galaxies with the same morphology. Apart from their brighter K-band magnitudes, we also find that their average SFR rate, star-formation efficiency, SFR and gas surface densities are larger than the respective values for normal spiral galaxies. At the same time though, the densities of the SFR and the gas follow the same relation as the one defined by normal galaxies. The SFR per unit luminosity decreases with the galaxy's luminosity, in agreement with a similar trend seen in normal galaxies. The galaxies under study are bright IRAS galaxies not just because they are intrinsically more luminous, but also because, on average, they have larger $L_{\rm FIR}/L_{\rm intr}$ ratio values than normal galaxies. Our results show also a correlation between $L_{\rm FIR}/L_{\rm intr}$ and F. This result suggests that the larger than "usual" $L_{\rm FIR}/L_{\rm intr}$ values are due to the fact that F, i.e. the fraction of the UV radiation which is reprocessed locally in HII regions, is larger than that in typical spirals. It is not clear though what the reason for this is, as we find no correlation between F and SFR (in absolute units), or M_K, or even surface densities of SFR and gas within the galaxies in the present sample.

Our dust-mass values range from 10^7 $M_\odot$ to 3×10^8 $M_\odot$. We find that the average gas-to-dust mass ratio of the galaxies in our sample is almost identical to the Galactic value, and that the average central face-on optical depth in the V band is 2.3, i.e. somewhat larger than unity. This result implies that the innermost parts of these galaxies would not be transparent in the optical part of the spectrum if they were seen face-on. This large optical depth though may not be representative of the whole spiral-galaxy population. Our results suggest that the gas surface density correlates positively with the dust surface density. Since these galaxies have a gas surface density which, on average, is larger than the gas surface density of normal spiral galaxies, we expect the same trend to hold for their dust surface density, and hence for τ_V as well. Furthermore, the optical depth we derived depends on the dust mass which in turn depends on the adopted dust cross section per unit mass, as we discussed in Sect. 6.2. If σ_{850} is indeed larger than the adopted value of 0.505 cm^2 gr^{-1}, then the computed τ_V values should decrease proportionally.

Finally, using the model derived SFR and dust-mass estimates, we find diagnostic relations between SFR and $L_{\rm FIR}$ or L_{100}, and between $M_{\rm d}$ and L_{850}. We believe that the SFR vs. $L_{\rm FIR}$ or L_{100} relations can be used to estimate (within a factor of ~2) the SFR of a galaxy with morphological type $0 \leq T \leq 6$ and $M_K \leq -23$. As for the $M_{\rm d}$ vs. L_{850} relation, the uncertainty of the derived $M_{\rm d}$ values depends on the uncertainty associated with the cross section per unit mass of the dust at 850 μm.

Acknowledgements. We wish to thank C. Popescu and R. Tuffs for taking the time to read this manuscript and give us their comments. This publication makes use of data products from the Two Micron All Sky Survey, which is a joint project of the University of Massachusetts and the Infrared Processing and Analysis Center/California Institute of Technology, funded by the National Aeronautics and Space Administration and the National Science Foundation. This research has made use of the NASA/IPAC Extragalactic Database (NED) which is operated by the Jet Propulsion Laboratory, California Institute of Technology, under contract with the National Aeronautics and Space Administration. Finally we would like to thank the referee V. Buat for her useful comments and suggestions.

References

Alton, P. B., Bianchi, S., Rand, R. J., et al. 1998, ApJ, 507, L125
Alton, P. B., Lequex, J., Bianchi, S., et al. 2001, A&A, 366, 541
Alton, P. B., Xilouris, E. M., Bianchi, S., Davies, J., & Kylafis, N. 2000, A&A, 356, 795
Bell, E. F. 2003, ApJ, 586, 794
Bell, E. F., Gordon, K. D., Kennicutt, R. C. Jr., & Zaritski, D. 2002, ApJ, 565, 994
Bendo, G. J., Joseph, R. D., Wells, M., et al. 2003, AJ, 125, 2361
Bianchi, S., Davies, J. I., & Alton, P. A. 1999, A&A, 344, L1
Bianchi, S., Davies, J. I., & Alton, P. A. 2000, A&A, 359, 65
Bianchi, S., Gonçalves, J., Albrecht, M., et al. 2003, A&A, 399, L43
Boselli, A., Tuffs, R. J., Gavazzi, G., Hippelein, H., & Pierini, D. 1997, A&AS, 121, 507
Bottinelli, L., Gouguenheim, L., Fouqué, P., & Paturel, G. 1990, A&AS, 82, 391
Böttner, C., Klein, U., & Heithausen, A. 2003, A&A, 408, 493
Bruzual, G., & Charlot, S. 2003, MNRAS, submitted
Buat, V., & Xu, C. 1996, A&A, 306, 61
Buat, V., Boselli, A., Gavazzi, G., & Bonfanti, C. 2002, A&A, 383, 801
Calzetti, D. 2001, PASP, 113, 1449
Casoli, F., Dickey, J., Kazës, I., et al. 1996, A&AS, 116, 193
Chan, G., & Fich, M. 1995, AJ, 109, 2611
Charlot, S., Kauffmann, G., Longhetti, M., et al. 2002, MNRAS, 330, 876
Chini, R., Kreysa, E., Mezger, P. G., & Gemund, H.-P. 1986, A&A, 154, L8
Chini, R., Krügel, E., & Lemke, R. 1996, A&AS, 118, 47
Davies, J. I., Alton, P., Trewhella, M., Evans, R., & Bianchi, S. 1999, MNRAS, 304, 495
de Jong, R. 1996, A&A, 313, 377 (DJ96)
de Vaucouleurs, G., de Vaucouleurs, A., Corwin, H. G. Jr., et al. 1991, Third Reference Catalogue of Bright Galaxies (Berlin, Heidelberg, New York: Springer-Verlag)

Devereux, N. A., & Young, J. S. 1990, ApJ, 359, 42
Dupac, X., del Burgo, C., Bernard, J.-P., et al. 2003, MNRAS, 344, 105
Devriendt, J. E. G., Guiderdoni, B., & Sadat, R. 1999, A&A, 350, 381
Dunne, L., Eales, S., Edmunds, M., et al. 2000, MNRAS, 315, 115 (DU00)
Dunne, L., & Eales, S. 2001, MNRAS, 327, 697
Efstathiou, A., & Rowan-Robinson, M. 2003, MNRAS, 343, 322
Elias, J. H., Frogel, J. A., Matthews, K., & Neugebauer, G. 1982, AJ, 87, 1029
Fioc, M., & Rocca-Volmerange B. 1997, A&A, 326, 950
Gavazzi, G., Pierini, D., & Boselli, A. 1996, A&A, 312, 397
Graham, A. W. 2001, MNRAS, 326, 543
Haas, M., Lemke, D., Stickel, M., et al. 1998, A&A, 338, L33
Hippelein, H., Haas, M., Tuffs, R. J., et al. 2003, A&A, 407, 137
Hirashita, H., Buat, V., & Inoue, A. K. 2003, A&A, 410, 83
Huchtmeier, W. K., & Richter, O.-G. 1989, A General Catalog of H_I Observations of Galaxies: The Reference Catalog (Berlin: Springer-Verlag)
Irwin, J. A., Stil, J. M., & Bridges, T. J. 2001, MNRAS, 328, 359
James, A., Dunne, L., Eales, S., & Edmunds, M. G. 2002, MNRAS, 335, 753
Kennicutt, R. C. Jr. 1998a, ApJ, 498, 541
Kennicutt, R. C. Jr. 1998b, ARA&A, 36, 189
Kuchinski, L. E., Terndrup, D. M., Gordon, K. D., & Witt, A. N. 1998, AJ, 115, 1438
Kylafis, N. D., & Bahcall, J. N. 1987, ApJ, 317, 637
Lavezzi, T. E., & Dickey, J. M. 1998, AJ, 115, 405
Lehnert, M. D., & Heckman, T. M. 1996, ApJ, 472, 546
Lisenfeld, U., Isaak, K. G., & Hills, R. 2000, MNRAS, 312, 433
Lisenfeld, U., Israel, F. P., Stil, J. M., & Sievers, A. 2002, A&A, 382, 860
Maiolino, R., Ruiz, M., Rieke, G. H., & Papadopoulos, P. 1997, ApJ, 485, 552
Mathis, J. S., & Whiffen, G. 1989, ApJ, 341, 808
Meurer, G. R., Heckman, T. M., Lehnert, M. D., Leitherer, C, & Lowenthal, J. 1997, AJ, 114, 54
Misiriotis, A., Popescu, C. C., Tuffs, R. J., & Kylafis, N. D. 2001, A&A, 372, 775
Möllenhoff, C., & Heidt, J. 2001, A&A, 368, 16
Ohta, K., & Kodaira, K. 1995, PASJ, 47, 17
Ossenkopf, V., & Henning, Th. 1994, A&A, 291, 943
Panuzzo, P., Bressan, A., Granato, G. L., Silva, L., & Danese, L. 2003, A&A, 409, 99
Pohlen, M., Dettmar, R.-J., & Lutticke, R. 2000, A&A, 357, 1
Popescu, C. C., Misiriotis, A., Kylafis, N. D., Tuffs, R. J., & Fischera, J. 2000, A&A, 362, 138 (P00)
Popescu, C. C., & Tuffs, R. J. 2002, MNRAS, 335, L41
Popescu, C. C., Tuffs, R. J., Kylafis, N. D., & Madore, B. F. 2003, A&A, in press
Popescu, C. C., Tuffs, R. J., Völk, H. J., Pierini, D., & Madore, B. F., 2002, ApJ, 567, 221
Sanders, D. B., & Mirabel, I. F. 1985, ApJ, 298, L31
Sanders, D. B., Scoville, N. Z., & Soifer, B. T. 1991, ApJ, 370, 158
Sanders, D. B., Young, J. S., Soifer, B. T., Schloerb, F. P., & Rice, W. L. 1986, ApJ, 305, L45
Silva, L., Granato, G. L., Bressan, A., & Danese, L. 1998, ApJ, 509, 103
Soifer, B. T., Boehmer, L., Neugebauer, G., & Sanders, D. B. 1989, AJ, 98, 766
Solomon, P. M., Downes, D., Radford, S. J. E., & Barrett, J. W. 1997, ApJ, 478, 144
Spignolio, L., Malkan, M. A., Rush, B., Carrasco, L., & Recillas-Cruz, E. 1995, ApJ, 453, 616
Theureau, G., Bottinelli, L., Coudreau-Durand, N., et al. 1998, A&AS, 130, 333
Trewhella, M., Davies, J. I., Alton, P. B., Bianchi, S., & Madore, B. F. 2000, ApJ, 543, 153
Tuffs, R. J., Popescu, C. C., Pierini, D., et al. 2002, ApJS, 139, 37
Weingartner, J. C., & Draine, B. T. 2001, ApJ, 548, 296
Xilouris, E. M., Kylafis, N. D., Papamastorakis, J., Paleologou, E. V., & Haerendel, G. 1997, A&A, 325, 135
Xilouris, E. M., Alton, P. B., Davies, J. I., et al. 1998, A&A, 331, 894
Xilouris, E. M., Byun, Y. I., Kylafis, N. D., Paleologou, E. V., & Papamastorakis, J. 1999, A&A, 344, 868
Xu, C., & Buat, V. 1995, A&A, 293, L65
Young, J. S., Xie, S., Tacconi, L., et al. 1995, ApJS, 98, 219